

MS. No.S-2017-012

# Stability of Slender Wall Boundaries Subjected to Earthquake Loading

by Pablo F. Parra and Jack P. Moehle

*Global instability of slender reinforced concrete walls occurs when the concrete section buckles out-of-plane over a portion of the wall length and height. Theoretical and numerical analyses were conducted on axially loaded prismatic members to evaluate the onset of global instability under tension/compression load cycles. A buckling theory suitable for hand calculations is introduced and evaluated using data available in the literature from tests conducted on columns. Computer simulations using force-based nonlinear elements with fibers are used to numerically simulate the tests and to study the influence of non-uniform strain profiles along the height of the member. The study shows that the onset of buckling can be identified using either the proposed buckling theory or finite element models. Furthermore, buckling is affected by gradients of axial load or strain along the length of the member. Design recommendations are made to inhibit global wall buckling during earthquakes.*

**Keywords:** buckling; earthquake; reinforced concrete; slenderness; wall boundary element.

## INTRODUCTION

Out-of-plane buckling of structural walls was reported following the 2010 Mw 8.8 Maule, Chile earthquake<sup>1-3</sup> and the 2011 Mw 6.3 New Zealand earthquake.<sup>4,5</sup> Figure 1 illustrates an example from a building in Chile. These observations created a renewed interest in research to better understand inelastic buckling of slender structural walls. The research included a review of past tests, analytical studies, and development of practical design guidance.

Lateral instability of walls or wall-like elements in laboratory tests has been reported previously. Oesterle et al.<sup>6</sup> first reported lateral instability leading to failure of a slender test wall with rectangular cross section. Goodsir<sup>7</sup> conducted a wall testing program to assess the effects of slenderness ratio and observed failure due to out-of-plane instability. Chai and Elayer<sup>8</sup> conducted tests of slender reinforced concrete columns, incrementing axial tension/compression cycles until buckling failure occurred. Thomsen and Wallace<sup>9</sup> reported the global instability of the slender stem of a T-shaped wall. In all the previously cited tests, the test specimens had two curtains of longitudinal reinforcement. Rosso et al.<sup>10</sup> reported global instability in the boundaries of two thin reinforced concrete walls with single layers of vertical and horizontal reinforcement.

In their review of test results, Oesterle et al.<sup>6</sup> observed that prior tensile cracking and plastic elongation of the wall boundaries for loading in one direction had reduced the effective stiffness of the wall, thereby reducing out-of-plane buckling resistance when loaded in the opposite direction.



*Fig. 1—Buckled wall at first story of a 15-story building following the 2010 Chile earthquake.*

This behavior is illustrated qualitatively in Fig. 2. Paulay and Priestley<sup>11</sup> described the mechanics of buckling of a boundary element that had been previously yielded in tension and developed a design recommendation that related the critical slenderness ratio to the mechanical reinforcement ratio and displacement ductility ratio. Chai and Elayer<sup>8</sup> extended the model based on observations from their column tests. Dashti et al.<sup>12</sup> used finite element models to simulate observed behavior of walls, including out-of-plane instability. More recently, Dashti et al.<sup>13</sup> presented experimental results of out-of-plane behavior in complete walls.

The present study reviews the mechanics of out-of-plane buckling of prismatic reinforced concrete elements and derives an expression relating critical slenderness ratio to the maximum tensile strain prior buckling during load

*ACI Structural Journal*, V. 114, No. 6, November-December 2017.

MS No. S-2017-012.R, doi: 10.14359/516851700836, received January 13, 2017, and reviewed under Institute publication policies. Copyright © 2017, American Concrete Institute. All rights reserved, including the making of copies unless permission is obtained from the copyright proprietors. Pertinent discussion including author's closure, if any, will be published ten months from this journal's date if the discussion is received within four months of the paper's print publication.

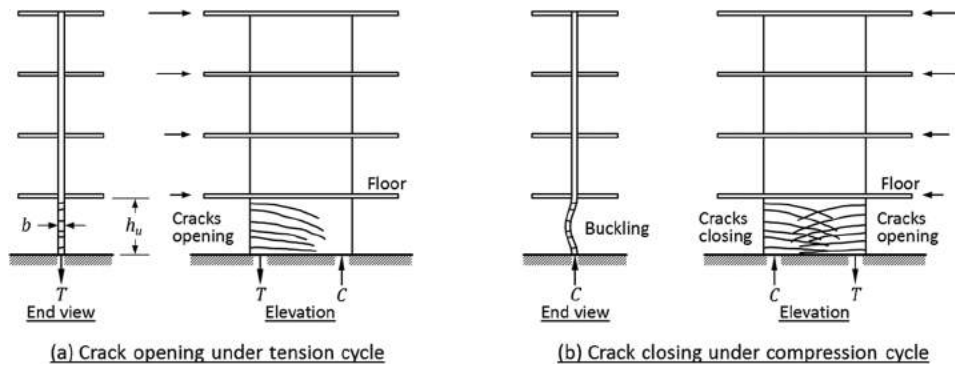


Fig. 2—Cracks under tension and compression cycles, after Chai and Elayer.<sup>8</sup>

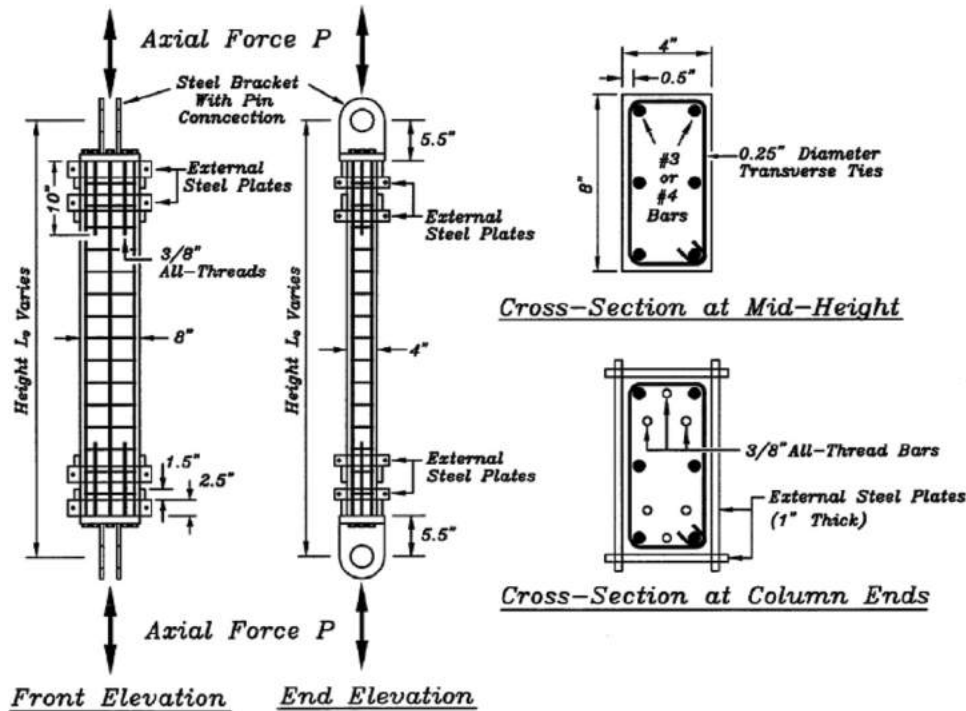


Fig. 3—Reinforcement details for test specimens, after Chai and Elayer.<sup>8</sup> (Note: 1 in. = 25.4 mm.)

reversal. The results of the model are compared with results of laboratory tests available in the literature<sup>8</sup> and OpenSees simulations of isolated columns. The combined results lead to a design recommendation for wall slenderness to inhibit out-of-plane instability. Boundary elements modeled as isolated columns have boundary conditions that are different from those in actual walls, which is a limitation of this study that can be addressed in future research.

### RESEARCH SIGNIFICANCE

The study derives and demonstrates a practical engineering approach that can be used to evaluate the buckling susceptibility of a slender structural wall or to establish design limits to inhibit lateral buckling.

### SLENDER COLUMN TESTS

Several tests have been performed<sup>8,14,15</sup> on prismatic reinforced concrete sections loaded under alternating tension and compression cycles, with the aim being to better understand instability of wall boundary elements. The 14 tests reported by Chai and Elayer<sup>8</sup> are especially relevant, as the maximum

tensile strain was gradually increased during each cycle until global buckling occurred during load reversal. These tests are used for evaluation of analytical models presented later in this paper. Figure 3 shows the reinforcement details for the test specimens. All specimens had pin-ended boundary conditions ( $k = 1$ ). Normalweight concrete was used in specimens with a compressive strength of 4950 psi (34.1 MPa). Yield strengths of the longitudinal reinforcement were 51.8 and 66.0 ksi (375 and 455 MPa) for No. 3 and No. 4 (No. 10 and No. 13) bars, respectively, and yield strength of the transverse ties was 99.0 ksi (683 MPa). Table 1 summarizes variables of the test program.

The test specimens were subjected to alternating axial tension and compression, where the axial maximum tensile strain was gradually increased in each cycle. For tensile strains exceeding the yield strain, crack closure would not occur after removal of the tensile force. Under subsequent compressive loading, the test specimens developed out-of-plane displacements, presumably due to irregular closure of the cracks. Eventually, the combination of axial compression and out-of-plane deformation resulted in crushing of the concrete on the

flexural compression face, leading to global buckling failure. Figure 4 shows the buckled shape of two specimens.

### ANALYTICAL MODEL FOR BUCKLING

As discussed by Oesterle et al.,<sup>6</sup> Paulay and Priestley,<sup>11</sup> and Chai and Elayer,<sup>8</sup> lateral instability of earthquake-resisting walls is determined by a complex interplay among wall geometry, material properties, and loading history. Under earthquake loading, the wall boundaries will be subjected to alternating tension and compression (Fig. 2). If the longitudinal reinforcement in the boundary yields in tension, the wall boundary cracks, with the residual crack width dependent on the amplitude of the reinforcement tensile strain  $\epsilon_{sm}$  during the tension excursion. This cracked section has reduced stiffness, which increases the tendency for wall instability when the section is subsequently subjected to compression.

The kinematics and equilibrium of a wall boundary with out-of-plane deformation can be derived with reference to

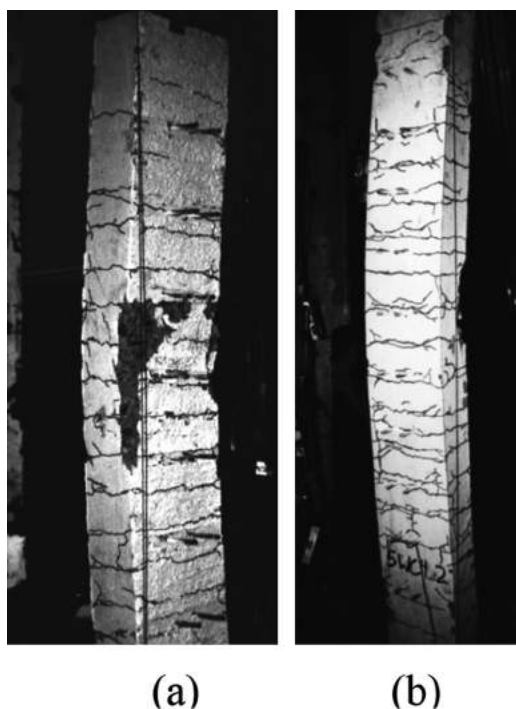


Fig. 4—Buckled shape for column with: (a)  $L_0/b = 14.75$ ; and (b)  $L_0/b = 17.75$ , after Chai and Elayer.<sup>8</sup>

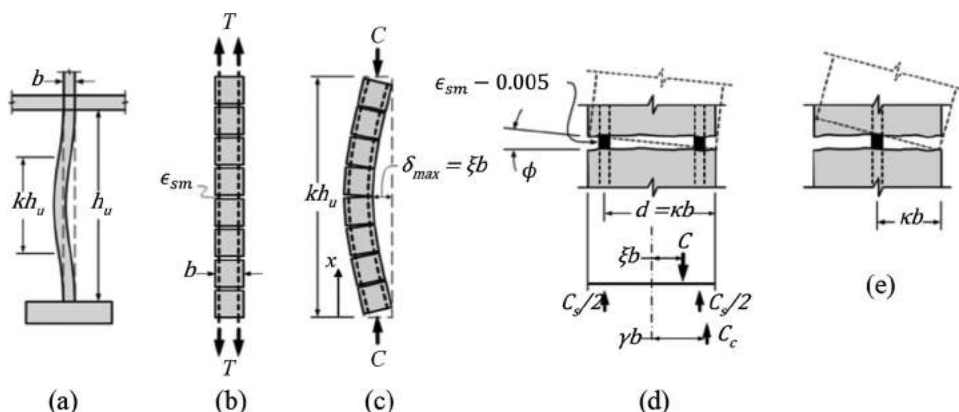


Fig. 5—Lateral instability of wall boundary previously yielded in tension, partly after Paulay and Priestley.<sup>11</sup>

Fig. 5, modified from Paulay and Priestley.<sup>11</sup> One assumes that the wall boundary is first subjected to some maximum tensile strain  $\epsilon_{sm}$  larger than the yielding strain  $\epsilon_y$ , such that crack closure under force reversal can only be achieved by yielding the longitudinal bars in compression (Fig. 5(b)). In a wall with two curtains of reinforcement, any slight asymmetry in the reinforcement or the loading will cause one curtain to yield before the other, leading to out-of-plane curvature (Fig. 5(c) and 5(d)). In a wall with one curtain of reinforcement, out-of-plane curvature can occur without yielding the longitudinal reinforcement (Fig. 5(e)).

To estimate conditions for stability, the effective height must be defined. The unbraced height is the clear story height  $h_u$  (Fig. 5(a)). For a multi-story wall with length  $l_w$  not less than the first-story clear height  $h_u$ , tensile yielding due to in-plane moment is likely to spread over a height not less than the clear story height  $h_u$ . Thus, it is reasonable to assume that the region susceptible to lateral buckling extends over the height  $h_u$ . In the present derivation, it is also assumed that the framing elements (or foundation) are sufficiently stiff to represent effectively fixed boundaries to the slender wall element. Thus, the effective height of the wall boundary is  $kh_u = 0.5h_u$  (Fig. 5(a) and 5(c)).

If it is assumed that the buckled shape follows a sine function (approach first followed by Chai and Elayer<sup>8</sup>), the maximum curvature at midheight is given by

$$\phi_{max} = -\delta_{max} \left( \frac{\pi}{kl_u} \right)^2 \quad (1)$$

Table 1—Test matrix, after Chai and Elayer<sup>8</sup>

Height-to-thickness ratio $L_0/b$	Longitudinal reinforcement ratio, percent	Transverse reinforcement spacing, in. (mm)	No. of specimens tested	$\xi$
11.75	2.1	2.25 (57)	1	0.190
11.75	3.8	3.0 (76)	1	0.123
14.75	2.1	2.25 (57)	3	0.189
14.75	3.8	3.0 (76)	3	0.123
17.75	2.1	2.25 (57)	3	0.189
17.75	3.8	3.0 (76)	3	0.123

The maximum lateral displacement is defined as  $\delta_{max} = \xi b$  in Fig. 5(c). The relation between  $\delta_{max}$  and  $\phi_{max}$  is

$$\delta_{max} = \xi b = \phi_{max} \left( \frac{kh_u}{\pi} \right)^2 \quad (2)$$

For a wall with two curtains of reinforcement,  $\phi_{max}$  can be estimated from the geometry of the strain profile in Fig. 5(d). Note that, at the onset of buckling, the wall boundary unloaded from the tensile loading and has been reloaded partially in compression. It can be assumed that the two curtains of reinforcement will be at some residual tensile strain  $\epsilon_r$  when one of the curtains yields in compression and crack closure commences on that side of the wall. Precise determination of  $\epsilon_r$  is complicated by the highly nonlinear and path-dependent behavior of the reinforcement under deformation reversals, and some simplifications are considered herein. Upon deformation reversal after reaching the maximum tensile strain  $\epsilon_{sm}$ , just before the boundary element yields in compression, the longitudinal reinforcement will have unloaded by strain  $\epsilon_s = f_{sm}/E_s$  and reloaded in compression to  $-\epsilon_y$ , ignoring the Bauschinger effect, such that the residual tensile strain is approximately  $\epsilon_r = \epsilon_{sm} - f_{sm}/E_s - \epsilon_y$ . To simplify the model, the residual tensile strain is approximated as  $\epsilon_r \approx \epsilon_{sm} - 0.005$ .

At the instant of crack closure, the out-of-plane curvature is

$$\phi_{max} = \frac{\epsilon_r}{d} = \frac{\epsilon_{sm} - 0.005}{d} \quad (3)$$

With this approximation, Eq. (2) and (3) are combined to obtain

$$\xi b = \frac{\epsilon_{sm} - 0.005}{d} \left( \frac{kh_u}{\pi} \right)^2 \quad (4)$$

When the wall is subjected to in-plane loading, the flexural compressive force  $C$  acting through the out-of-plane displacement  $\xi b$  produces an out-of-plane moment  $C \times \xi b$ . If the out-of-plane moment strength is sufficient to resist this moment, the cracks will close through the thickness of the wall and the wall will be stabilized. Otherwise, the wall will experience out-of-plane moment failure and lateral instability failure. Based on these considerations, Paulay and Priestley<sup>11</sup> derived an expression for the critical value of out-of-plane displacement  $\xi_{cr} b$ , defined by

$$\xi_{cr} = 0.5 \left( 1 + \frac{2m}{0.85} - \sqrt{\left( \frac{2m}{0.85} \right)^2 + \frac{4m}{0.85}} \right) \quad (5)$$

in which  $m = \rho f_y / f_c$  is the mechanical reinforcement ratio.

Substituting  $\xi_{cr}$  for  $\xi$  for and  $\kappa b$  for  $d$  in Eq. (4), and then reorganizing terms, one obtains the critical ratio of thickness to effective height as

$$\frac{b_{cr}}{kh_u} = \frac{1}{\pi} \sqrt{\frac{\epsilon_{sm} - 0.005}{\kappa \xi_{cr}}} \quad (6)$$

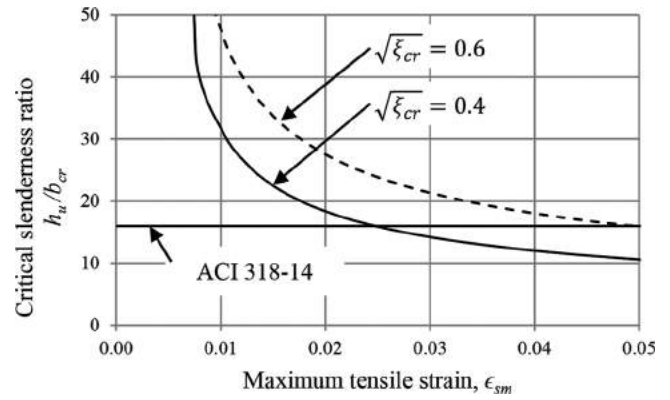


Fig. 6—Critical slenderness ratio as function of maximum tensile strain.

Alternatively, for given geometry, one can solve Eq. (6) for the maximum tensile strain  $\epsilon_{sm,cr}$  as

$$\epsilon_{sm,cr} = \kappa \xi_{cr} \left( \frac{\pi b_{cr}}{kh_u} \right)^2 + 0.005 \quad (7)$$

The main variables appearing in Eq. (6) and (7) are slenderness ratio  $k_{hu}/b_{cr}$ , maximum tensile strain  $\epsilon_{sm}$  in longitudinal reinforcement, effective depth parameter  $\kappa$  for longitudinal reinforcement, and  $\xi_{cr}$ . Parameter  $\kappa$  can be found from  $d = \kappa b$ , where it is noted that  $\kappa \approx 0.8$  for thin walls with two curtains of reinforcement and 0.5 for walls with a single layer of reinforcement. From this, it is clear that walls with two curtains of longitudinal reinforcement are inherently more stable than walls with a single curtain.

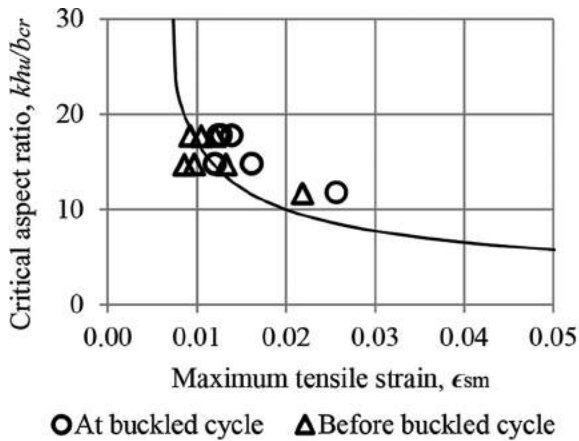
Equation (5) relates parameter  $\xi_{cr}$  with the mechanical reinforcement ratio  $m$ . For practical construction,  $0.4 \leq \sqrt{\xi_{cr}} \leq 0.6$  (corresponding to values of  $m$  between 0.31 and 0.02). Equation (6) is plotted in Fig. 6 for the two practical limit values of  $\sqrt{\xi_{cr}}$ ,  $\kappa = 0.8$ , and considering fixed-fixed boundary conditions ( $k = 0.5$ ). Also shown is the limiting slenderness ratio of boundary elements for special structural walls from ACI 318-14—that is,  $h_u/b_{cr} = 16$ .

Figure 7 plots results of Eq. (6) (continuous curves) and reported values of  $\epsilon_{sm}$  for the tests reported by Chai and Elayer.<sup>8</sup> The circle symbol corresponds to the maximum tensile strain in the final cycle where buckling failure occurred and the triangle symbol corresponds to the maximum tensile strain in the previous load cycle where the specimen was still stable. The results suggest that Eq. (6) is a good approximation of the test results.

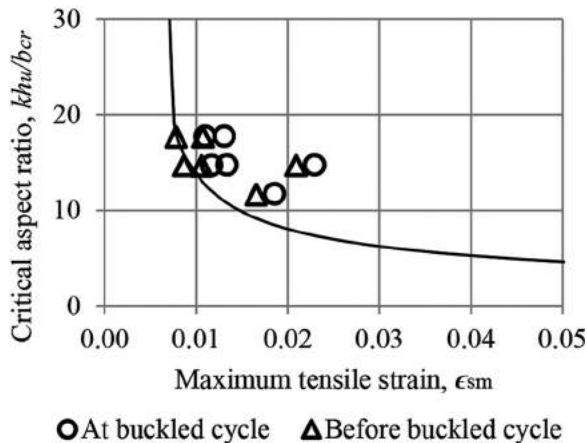
The parameter  $\xi$  defined in Eq. (6) is inconvenient for preliminary design. Selecting a value of  $\sqrt{\xi_{cr}} = 0.5$  (mid-value in the practical range), Eq. (6) can be simplified to

$$\frac{b_{cr}}{kh_u} = 0.7 \sqrt{\epsilon_{sm} - 0.005} \quad (8)$$

Equation (8) is now plotted in Fig. 8 with the results of all columns tested by Chai and Elayer.<sup>8</sup> The results suggest that Eq. (8) is a reasonable approximation to describe behavior of uniformly loaded prisms. If  $\epsilon_{sm}$  is limited to 0.03 (Rodriguez et al.<sup>16</sup>), and  $k = 0.5$  for fixed-fixed boundary conditions,



(a)



(b)

Fig. 7—Measured and estimated values of  $\epsilon_{sm}$ : (a)  $\rho = 2.1\%$ ; and (b)  $\rho = 3.8\%$ . Experimental data obtained from Chai and Elayer.<sup>8</sup>

Eq. (8) results in  $h_u/b_{cr} = 18.1$ . This compares with the ACI 318-14 limit of 16, as shown in Fig. 6.

### FINITE ELEMENT MODEL FOR BUCKLING: CONSTANT AXIAL FORCE

The analytical model introduced in the preceding section is suitable for modeling lateral instability of prismatic members under constant axial force. The finite element method can be used to study response under more generalized loadings. This begins by testing the finite element method for the case of constant axial force.

A finite element model was assembled using force-based nonlinear beam-column elements with fibers and corotational formulation to consider nonlinear geometry. The model was implemented in OpenSees.<sup>17</sup> The material object used for concrete is Concrete01. This is a uniaxial concrete model<sup>18-21</sup> with degraded linear unloading/reloading stiffness according to the work of Karsan and Jirsa<sup>22</sup> and no tensile strength. The uniaxial Giuffrè-Menegotto-Pinto<sup>23</sup> steel material object with isotropic strain hardening is used to model reinforcing bars (Steel02 material). This model can represent the hysteretic behavior of steel reinforcement exhibiting the Bauschinger

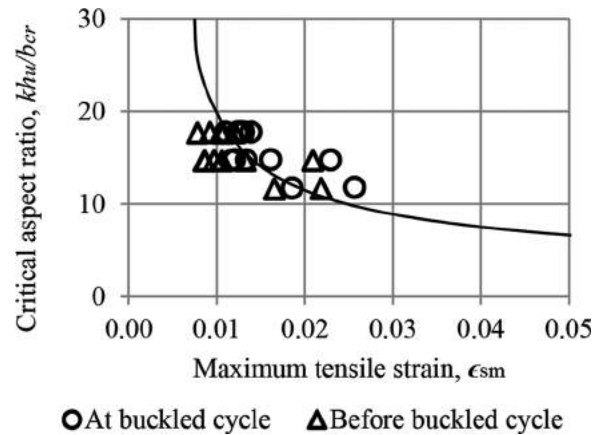


Fig. 8—Measured and estimated  $\epsilon_{sm}$  values according to Eq. (8). Experimental data obtained from Chai and Elayer.<sup>8</sup>

effect together with isotropic strain hardening. Perfect bond is assumed between steel and concrete.

Lateral instability during crack closure initiates because the application point of the external force may not coincide with the centroid of the resistant force in the reinforcement. There are several plausible explanations of why this occurs, including variations in reinforcement properties, irregularities in reinforcement placement, and earthquake loading effects in the orthogonal direction. To initiate instability in OpenSees, the authors reduced the yield stress in one layer of reinforcement by 1 ksi (7 MPa). Studies using yield stress reductions of 0.1, 0.3, 0.5, 0.7, and 1 ksi (0.7, 2, 3, 5, and 7 MPa) showed that behavior was insensitive to this parameter.<sup>3</sup>

Strain localization in force-based elements causes the response to be mesh-dependent. To address this behavior, the concrete material is regularized according to the procedure developed by Coleman and Spacone.<sup>24</sup> Material regularization allows maintaining objectivity of the structural response independent of the number of integration points selected for analysis.

To test sensitivity of the finite element results to the modeling assumptions, the authors developed various models of Chai and Elayer's Test Specimen 4WC3\_1 ( $L_0/b = 14.75$  with  $\rho = 2.1\%$ ).<sup>7</sup> The finite element model (Fig. 9) uses four force-based elements with four, five, or six integration points per element (Gauss-Lobatto quadrature). The concrete in each element is discretized into 11 fibers evenly distributed across the short dimension of the cross section. Longitudinal reinforcing bars are represented directly. The upper and lower limits for compressive fracture energy reported by Feenstra<sup>25</sup>—0.06 and 0.14 kip/in. (10 and 25 N/mm)—are considered. Table 2 summarizes the variables of the analysis.

The regularized concrete material introduced by Coleman and Spacone<sup>24</sup> considers a parabolic prepeak behavior followed by a linear postpeak softening branch until a stress of 20%  $f'_c$ 's is reached at a prescribed strain labeled  $\epsilon_{20}$ . The residual strength is assumed to remain constant for strains larger than  $\epsilon_{20}$ . Table 2 presents  $\epsilon_{20}$  for all analyzed cases.

Figure 10 compares the measured and calculated responses for Test Specimen 4WC3\_1. Figure 10(a) shows the nominal axial strain versus out-of-plane displacement normalized by the column width  $b$ , and Fig. 10(b) shows

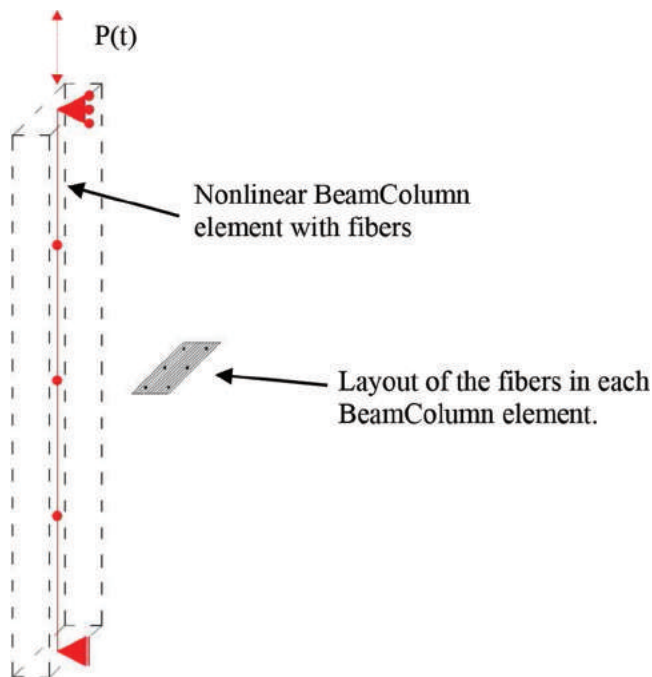


Fig. 9—OpenSees model for column instability.

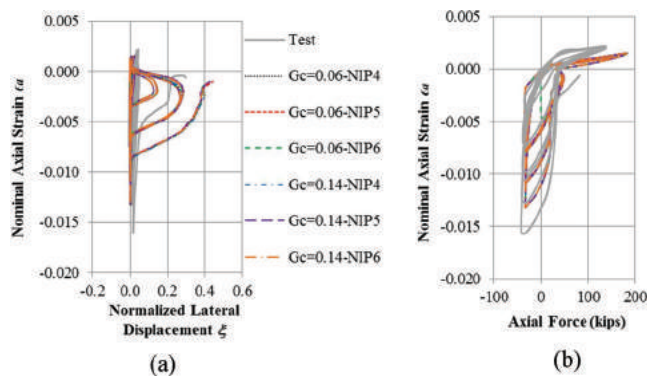


Fig. 10—Specimen 4WC3\_1, response sensitivity to compressive fracture energy and number of integration points. Experimental data obtained from Chai and Elayer.<sup>8</sup> (Note: 1 kip = 4.45 kN.)

**Table 2—Concrete ultimate strain according to Coleman and Spacone<sup>24</sup> regularization**

$G_c$ , kip/in. (N/mm)	Number of integration points	$\epsilon_{20}$
0.06 (10)	4	0.017
	5	0.027
	6	0.040
0.14 (25)	4	0.040
	5	0.066
	6	0.099

the nominal axial strain versus axial force. Compression variables have a positive sign. For peak tensile strains up to  $-0.0133$ , the measured out-of-plane displacements were less than  $0.05b$ . After loading to peak tensile strain close to  $-0.016$ , unloading toward compression resulted in a rapid increase in the out-of-plane displacement. The out-of-plane

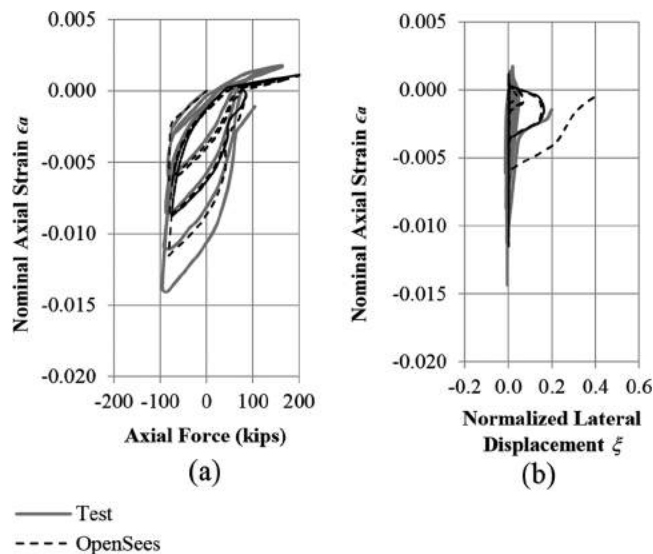


Fig. 11—Specimen 4WC4\_2, measured versus analytical response. Experimental data obtained from Chai and Elayer.<sup>8</sup> (Note: 1 kip = 4.45 kN.)

displacement resulted in crack closure on one side of the cross section followed by concrete crushing.

The calculated responses show larger out-of-plane displacements at lower tensile strains than were observed in the tests. “Crack” closure, however, resulted in straightening of the analytical model during these low-amplitude cycles. Instability failure was calculated to occur for tensile strain of  $-0.0133$ . It is interesting that the finite element model of this section and the analytical model of the preceding section both identify instability at a tensile strain less than that of the actual test.

The calculated responses shown in Fig. 10 are relatively insensitive to both the number of integration points and the compressive fracture energy, confirming that a mesh-independent structural response is achieved by regularizing the concrete material using the constant fracture energy approach. Therefore, for the following analyses, calculated results are shown only for models using four elements with four integrations points each and a constant fracture energy of 0.1 kip/in. (18 N/mm), which is at the middle of the plausible range reported by Feenstra.<sup>25</sup>

Figures 11, 12, and 13 compare the measured and calculated responses of Specimens 4WC4\_2 ( $L_0/b = 14.75$  with  $\rho = 3.8\%$ ), 5WC3\_2 ( $L_0/b = 17.75$  with  $\rho = 2.1\%$ ), and 5WC4\_3 ( $L_0/b = 17.75$  with  $\rho = 3.8\%$ ), respectively. Lateral instability failure is obtained in each of the analyses. Similar to results for 4WC3\_1, however, the OpenSees model underestimates the maximum tensile strain required to buckle the column during load reversal, and overestimates the maximum lateral displacement in cycles before failure.

### FINITE ELEMENT MODEL FOR GLOBAL BUCKLING: VARYING AXIAL FORCE

Figure 14(a) depicts a slender wall in a multi-story building with uniform story heights. The moment diagram is representative of moments occurring in a frame-wall structure under lateral loading. Given the relatively smaller variation

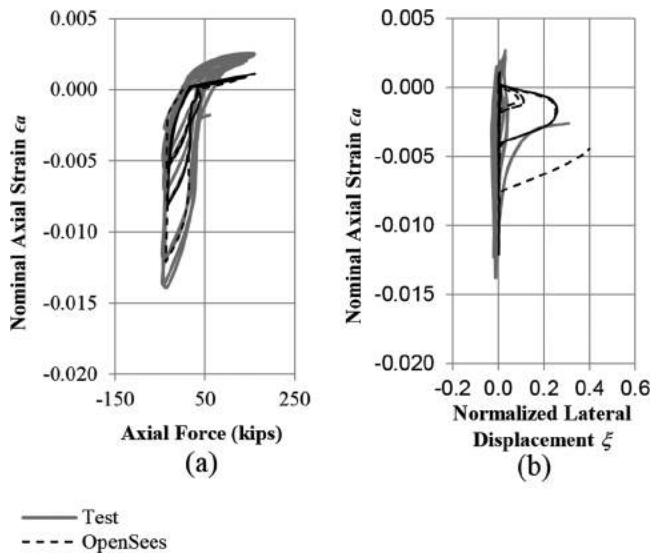


Fig. 12—Specimen 5WC3\_2, measured versus analytical response. Experimental data obtained from Chai and Elayer.<sup>8</sup> (Note: 1 kip = 4.45 kN.)

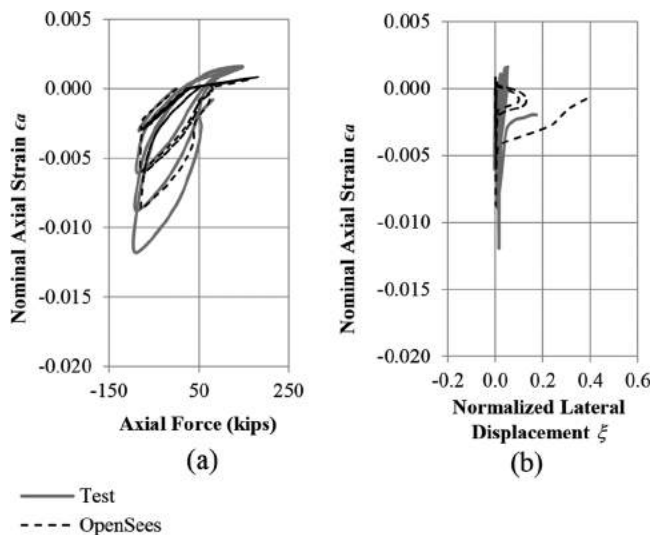


Fig. 13—Specimen 5WC4\_3, measured versus analytical response. Experimental data obtained from Chai and Elayer.<sup>8</sup> (Note: 1 kip = 4.45 kN.)

of moment over the first-story height, it might be reasonable to model the boundary element in that story as having constant axial force over height, as was done in previous sections of this paper. Figure 14(b) depicts the same wall, except it has a taller first story, resulting in greater variation of moment with the first story. In this case, the assumption of constant axial force may no longer be valid.

The effect of moment gradient or, alternatively, of axial force variation along the wall height, is evaluated in an idealized way using OpenSees models of isolated boundary elements, as shown in Fig. 15. Each boundary element is modeled like the model described previously, except using 10 evenly spaced nonlinear beam-column elements along the length. The analytical model is fixed at the base and free to translate vertically at the top without rotation. Axial force is applied through point forces at the nodes, following one of

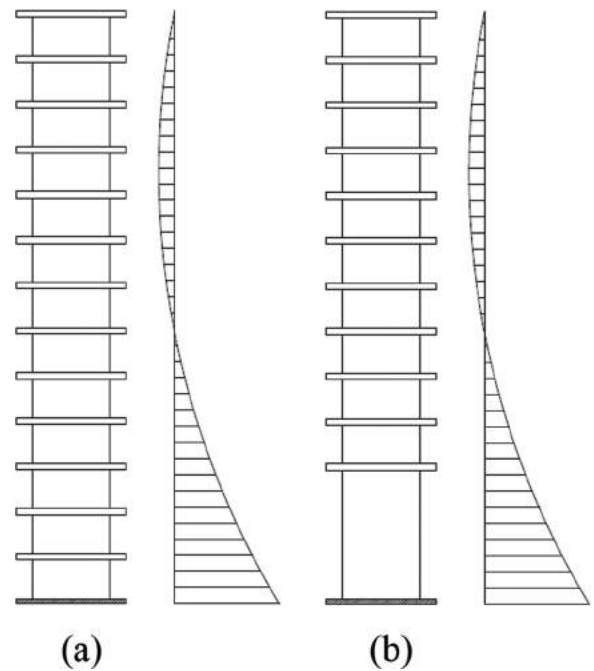


Fig. 14—Slender multi-story wall and moment diagram over the height: (a)  $M$  nearly constant in first story; and (b)  $M$  varies in first story.

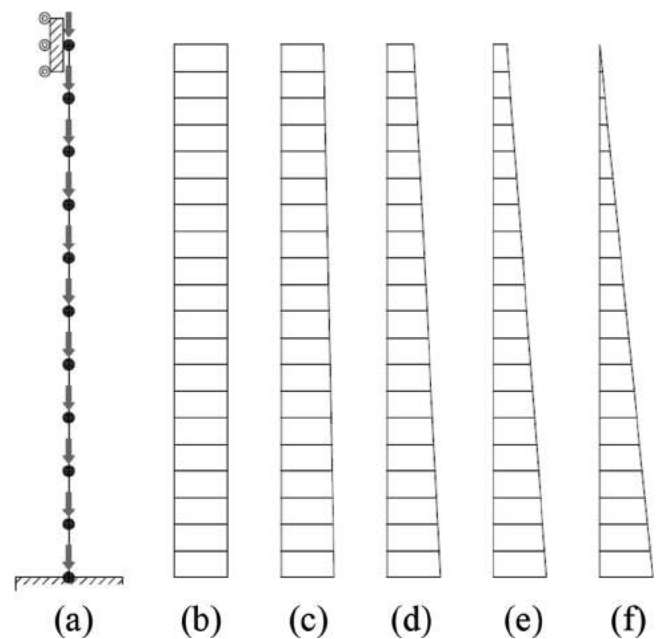


Fig. 15—(a) OpenSees model for boundary element, axial force gradient: (b)  $\alpha = 1$ ; (c)  $\alpha = 0.8$ ; (d)  $\alpha = 0.5$ ; (e)  $\alpha = 0.25$ ; and (f)  $\alpha = 0$ , where  $\alpha$  is the ratio between top and bottom axial force.

five different axial force distributions (Fig. 15(b) to 15(f)). A model is first loaded in tension to a target vertical displacement of  $-0.1$  in. ( $-2.5$  mm) at the top of the model, followed by loading in the opposite direction until the displacement at the top of the model is returned to zero. These cycles are repeated, but with the vertical displacement in tension incremented  $-0.1$  in ( $-2.5$  mm) in each cycle until achieving buckling failure during load reversal.

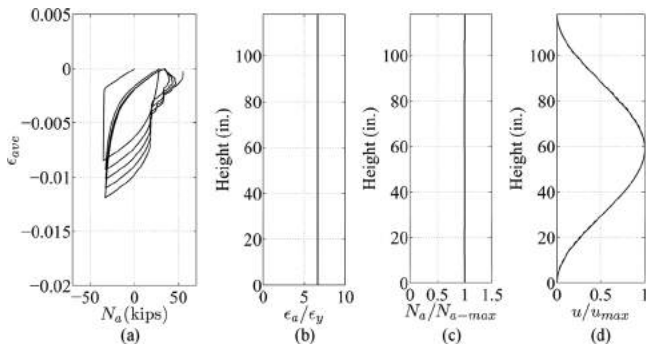


Fig. 16—Specimen 4WC3\_1,  $\alpha = 1$ : (a) average axial strain versus axial force at the base; (b) normalized axial strain; (c) normalized axial force; and (d) normalized buckled shape. (Note: 1 in. = 25.4 mm.)

The analyses are carried out for four of the test columns reported by Chai and Elayer<sup>8</sup> (Specimens 4WC3\_1, 4WC4\_2, 5WC3\_2, and 5WC4\_3). These columns were tested under pinned-pinned boundary conditions, in contrast with the fixed-fixed boundary conditions in the analytical model. Therefore, the unsupported height  $h_u$  for analytical models was set at  $2L_0$ , where  $L_0$  is the length of the column test specimen. The effective slenderness ratios were  $kh_u/b = 14.75$  and  $17.75$  for these cases. One additional case was considered analytically, having  $kh_u/b = 25$  and longitudinal steel ratio  $\rho = 2.1\%$ .

Figure 16 shows the analysis results for Specimen 4WC3\_1 with constant axial force over the height ( $\alpha = 0$ ). Four plots are provided: 1) the history of the average axial strain (top vertical displacement divided by the model height) versus axial force at the base, limited to cycles immediately preceding buckling; 2) the variation over height of axial strain normalized by the yielding strain,  $\epsilon_s/\epsilon_y$ , as measured during the maximum tensile excursion before buckling; 3) the normalized axial force distribution over height; and 4) a comparison between the calculated out-of-plane displaced shape (continuous line) and theoretical sine shape (discontinuous line) applicable to elastic buckling of a fixed-ended column. For this test case, maximum tensile strain prior to buckling is  $\epsilon_s \approx 7\epsilon_y$  (Fig. 16(b)) and the buckled shape obtained from OpenSees matches the theoretical sine curve expected for a fixed-ended column under uniform axial compression (Fig. 16(d)).

When the axial load is changed to a non-uniform profile like the one shown in Fig. 15(c), where  $\alpha = 0.8$ , the buckled shape obtained from analysis is no longer a sine curve. Instead, maximum out-of-plane displacements are shifted downward (Fig. 17(d)). The average elongation prior to buckling is slightly increased relative to the case where  $\alpha = 1.0$ , that is,  $\epsilon_{ave} = 0.013$  for  $\alpha = 0.8$  versus  $\epsilon_{ave} = 0.012$  for  $\alpha = 1.0$ . Note that the local strains are no longer constant over height, and the maximum value is nearly twice the value for  $\alpha = 1.0$ .

Figures 18 and 19 show how the maximum lateral displacement shifts toward the base, and maximum tensile strain increases, with decreasing value of  $\alpha$ .

The results of the preceding paragraphs are for Test Specimen 4WC3\_1. Similar results are obtained for the other cases that were studied.<sup>3</sup>

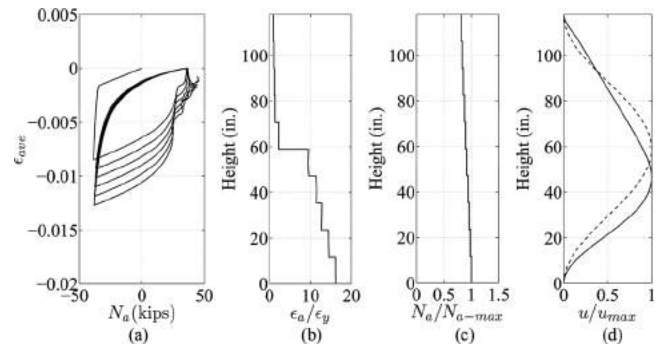


Fig. 17—Specimen 4WC3\_1,  $\alpha = 0.8$ : (a) average axial strain versus axial force at the base; (b) normalized axial strain; (c) normalized axial force; and (d) normalized buckled shape. (Note: 1 in. = 25.4 mm.)

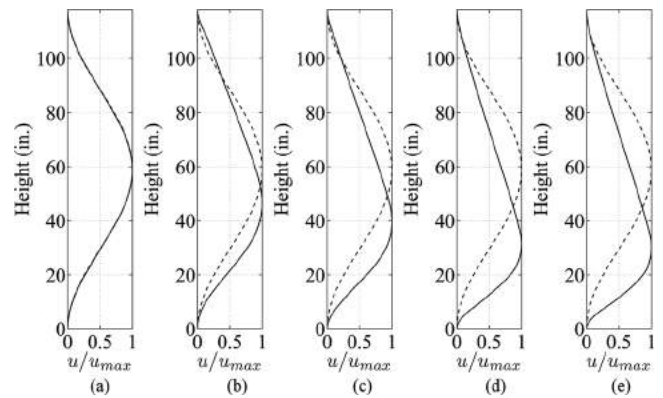


Fig. 18—Normalized out-of-plane displacement, theoretical shape (discontinuous line) versus OpenSees modeling ( $kh_u/b = 14.75$ ,  $\rho = 2.1\%$ ) for: (a) uniform axial force profile  $\alpha = 1$ ; (b)  $\alpha = 0.8$ ; (c)  $\alpha = 0.5$ ; (d)  $\alpha = 0.25$ ; and (e)  $\alpha = 0$ . (Note: 1 in. = 25.4 mm.)

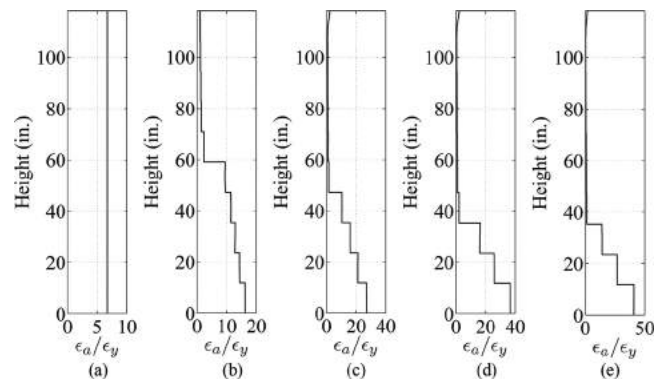


Fig. 19—Normalized tensile strain profile, prior buckling during load reversal, along the element height ( $kh_u/b = 14.75$ ,  $\rho = 2.1\%$ ) from OpenSees modeling for: (a) uniform axial force profile  $\alpha = 1$ ; (b)  $\alpha = 0.8$ ; (c)  $\alpha = 0.5$ ; (d)  $\alpha = 0.25$ ; and (e)  $\alpha = 0$ . (Note: 1 in. = 25.4 mm.)

Figure 20 shows the maximum local strain and average strain versus  $\alpha$  for all analyzed cases. Maximum local strain is defined as the maximum tensile strain prior to buckling along the column length, and average strain is defined as the total column elongation prior to buckling divided by its initial length. Both strains are normalized by their corre-

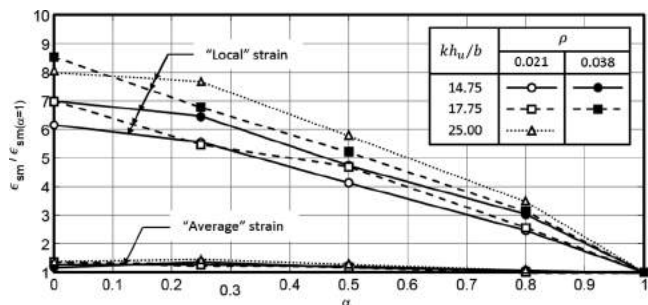


Fig. 20—Normalized maximum tensile strain during cycle before buckling versus  $\alpha$ .

sponding values for constant axial force over the height ( $\alpha = 1.0$ ). For all cases, the local strain increases monotonically with decreasing  $\alpha$ , that is, as the axial force gradient becomes steeper. This increment in the maximum local strain increases with increasing steel ratio and with increasing slenderness ratio. The average strain also increased with decreasing  $\alpha$ , although this increment is modest and can be neglected for practical purposes.

Analytical models for the assessment of nonlinear strains in structural walls commonly use either plastic hinge models or fiber models in which the fibers extend over a height on the order of the typical story height. For such models, the “average” strain results of Fig. 20 are applicable, indicating that the effect of  $\alpha$  can be ignored without undue conservatism. Therefore, the results of Eq. (6) can be conservatively applied. In buildings with unusually tall stories, as in a building with an atrium, the length of the plastic hinge or the height of the fiber may be only a small fraction of the unbraced clear height of the wall. Where this occurs, the applicability of Fig. 20 needs to be evaluated on a case-by-case basis.

## SUMMARY AND CONCLUSIONS

Past earthquakes and laboratory tests have shown the vulnerability of slender structural walls to lateral instability. An analytical study was carried out to understand the primary variables that affect instability, with the following conclusions:

1. The tendency of a structural wall to buckle under cyclic loading depends mainly on: a) the slenderness ratio  $kh_u/b$  of the wall boundary; b) the maximum tensile strain experienced by the member prior to axial compression; and c) whether the wall as one or two curtains of reinforcement.

2. An analytical model for buckling of prismatic members with two curtains of reinforcement under uniform tension/compression cycles is used to derive an equation to identify walls that are susceptible to lateral instability. The model produces results that compare well with results obtained from laboratory tests.

3. Lateral instability of prismatic members subjected to cyclic lateral loading can be simulated using finite-element computer software using nonlinear beam/column elements.

4. Structural loading can produce tensile and compressive stresses that vary approximately linearly from some

maximum value at the bottom to some smaller value at the top of the clear height. For such members, the variable axial force produces a buckled shape that is shifted toward the base. Maximum local tensile strain prior to onset of buckling increases as the axial force gradient increases. Tensile strain averaged over the clear height, however, does not increase significantly.

5. In multi-story buildings with story heights not significantly different from the typical story height, it is reasonable to estimate the tendency for lateral instability using the average strain over the plastic hinge length or the typical story height, regardless of moment gradients over the first-story height.

## AUTHOR BIOS

**Pablo F. Parra** is an Assistant Professor of Civil Engineering at Universidad Adolfo Ibáñez, Chile. He received his MS and PhD in civil and environmental engineering from University of California, Berkeley, CA.

**Jack P. Moehle**, F.A.C.I., is the Ed & Diane Wilson Presidential Professor of Structural Engineering at the University of California, Berkeley. He is the Chair of the ACI Committee 318, Structural Concrete Building Code. His research interests include design and analysis of structural systems, with an emphasis on earthquake engineering, reinforced concrete construction, new and existing buildings and infrastructure, and development of professional design guidance.

## ACKNOWLEDGMENTS

This research has been supported by the National Institute of Standards and Technology through the ATC 94 project. Their support is gratefully acknowledged. Opinions, findings, conclusions and recommendations are those of the authors and do not necessarily represent those of the sponsor. The first author would like to thank Comisión Nacional de Investigación Científica y Tecnológica (CONICYT, Chile) and the Fulbright Student Program for providing necessary financial assistance to pursue his PhD at the University of California, Berkeley.

## NOTATION

$A_g$	=	gross area of the specimen
$b$	=	wall width
$b_{cr}$	=	critical wall width
$c$	=	neutral axis depth
$C$	=	compressive force (Fig. 3)
$C_c$	=	compressive force in concrete (Fig. 3)
$C_s$	=	compressive force in reinforcement (Fig. 3)
$d$	=	effective depth of boundary element (Fig. 3)
$E_c$	=	reinforcement Young's modulus
$f'_c$	=	specified compressive strength of concrete
$f'_{sm}$	=	maximum tensile stress in boundary element reinforcement
$f_y$	=	reinforcement yield stress
$G_c$	=	concrete compressive fracture energy
$h_u$	=	unsupported height
$k$	=	effective length factor
$L_0$	=	length of the column specimen
$l_w$	=	horizontal length of the wall section
$m$	=	mechanical reinforcement ratio $\rho f_y / f'_c$
$N_a$	=	axial force in boundary element
$T$	=	tension force in boundary element
$\alpha$	=	ratio of axial force at the boundary element top to axial force at the bottom
$\beta_1$	=	ratio of depth of rectangular stress block to neutral axis depth
$\gamma$	=	relative position of concrete compressive force $C_c$ (Fig. 3)
$\delta_{max}$	=	wall maximum lateral deflection
$\epsilon_{res}$	=	reinforcement residual tensile strain
$\epsilon_{sm}$	=	maximum tensile strain in boundary element reinforcement
$\epsilon_y$	=	reinforcement yield strain
$\kappa$	=	ratio $d/b$
$\xi$	=	ratio $\delta_{max}/b$
$\rho$	=	ratio of boundary element reinforcement
$\phi_{max}$	=	maximum curvature at the boundary element midheight (Fig. 3)

## REFERENCES

1. ATC-94, "Recommendations for Seismic Design of Reinforced Concrete Wall Buildings Based on Studies of the 2010 Chile Earthquake," Applied Technology Council, Redwood City, CA, 2014.
2. Parra, P. F., and Moehle, J. P., "Lateral Buckling in Reinforced Concrete Walls," *Tenth U.S. National Conference on Earthquake Engineering*, Anchorage, AK, 2014. doi:10.4231/D3V40K05Q.10.4231/D3V40K05Q
3. Parra, P. F., "Stability of Reinforced Concrete Wall Boundaries," PhD dissertation, Civil and Environmental Engineering Department, University of California, Berkeley, Berkeley, CA, 2016, 219 pp.
4. Sritharan, S.; Beyer, K.; Henry, R. S.; Chai, Y. H.; Kowalsky, M.; and Bull, D., "Understanding Poor Seismic Performance of Concrete Walls and Design Implications," *Earthquake Spectra*, V. 30, No. 1, 2014, pp. 307-334. doi: 10.1193/021713EQS036M
5. Kam, W.; Pampanin, S.; and Elwood, K., "Seismic Performance of Reinforced Concrete Buildings in the 22 February Christchurch (Lyttelton) Earthquake," *Bulletin of the New Zealand Society for Earthquake Engineering*, V. 44, No. 4, 2011, pp. 239-278.
6. Oesterle, R. G.; Fiorato, A. E.; Johal, L. S.; Carpenter, J. E.; Russell, H. G.; and Corley, W. G., "Earthquake Resistant Structural Walls—Tests of Isolated Walls," Portland Cement Association, Skokie, IL, 1976, 318 pp.
7. Goodsir, W. J., "The Design of Coupled Frame-Wall Structures for Seismic Actions," University of Canterbury, Christchurch, New Zealand, 1985, 387 pp.
8. Chai, Y. H., and Elayer, D. T., "Lateral Stability of Reinforced Concrete Columns under Axial Reversed Cyclic Tension and Compression," *ACI Structural Journal*, V. 96, No. 5, Sept.-Oct. 1999, pp. 780-789. doi: 10.14359/732
9. Thomsen, J. H. IV, and Wallace, J. W., "Displacement-Based Design of Slender Reinforced Concrete Structural Walls—Experimental Verification," *Journal of Structural Engineering*, ASCE, V. 130, No. 4, 2004, pp. 618-630. doi: 10.1061/(ASCE)0733-9445(2004)130:4(618)
10. Rosso, A.; Almeida, J. P.; and Beyer, K., "Stability of Thin Reinforced Concrete Walls under Cyclic Loads: State-of-the-Art and New Experimental Findings," *Bulletin of Earthquake Engineering*, V. 14, No. 2, 2016, pp. 455-484. doi: 10.1007/s10518-015-9827-x
11. Paulay, T., and Priestley, M., "Stability of Ductile Structural Walls," *ACI Structural Journal*, V. 90, No. 4, July-Aug. 1993, pp. 385-392. doi: 10.14359/3958
12. Dashti, F.; Dhakal, R. P.; and Pampanin, S., "Numerical Simulation of Shear Wall Failure Mechanisms," 2014 NZSEE Conference, Auckland, New Zealand, 2014, pp. 1-12.
13. Dashti, F.; Dhakal, R.; and Pampanin, S., "An Experimental Study on Out-of-Plane Deformations of Rectangular Structural Walls Subject to In-Plane Loading," 16th World Conference on Earthquake Engineering, Santiago, Chile, 2017.
14. Creagh, A.; Acevedo, C.; Moehle, J. P.; Hassan, W.; and Tanyeri, A. C., "Seismic Performance of Concrete Special Boundary Element," Network for Earthquake Engineering Simulation, Arlington, VA, 2010, 18 pp.
15. Acevedo, C. E.; Creagh, A.; Moehle, J. P.; Hassan, W.; and Tanyeri, A. C., "Seismic Vulnerability of Non-Special Boundary Element of Shear Wall under Axial Force Reversals," Network for Earthquake Engineering Simulation, Arlington, VA, 2010, 16 pp.
16. Rodriguez, M. E.; Botero, J. C.; and Villa, J., "Cyclic Stress-Strain Behavior of Reinforcing Steel Including Effect of Buckling," *Journal of Structural Engineering*, ASCE, V. 125, No. 6, 1999, pp. 605-612. doi: 10.1061/(ASCE)0733-9445(1999)125:6(605)
17. Mazzoni, S.; McKenna, F.; Scott, M. H.; and Fenves, G., "Open System for Earthquake Engineering Simulation: User Command-Language Manual," Pacific Earthquake Engineering Research Center, University of California, Berkeley, Berkeley, CA, 2007.
18. Kent, D. C., and Park, R., "Flexural Members with Confined Concrete," *Journal of the Structural Division*, V. 97, 1971, pp. 1969-1990.
19. Scott, B. D.; Park, R.; and Priestley, M. J. N., "Stress-Strain Relationships for Confined Concrete: Rectangular Sections," *Research Report*, University of Canterbury, New Zealand, 1980, 106 pp.
20. Hognestad, E., "Study of Combined Bending and Axial Load in Reinforced Concrete Members," College of Engineering, Engineering Experiment Station, University of Illinois at Urbana-Champaign, Champaign, IL, 1951.
21. Roy, H. E. H., and Sozen, M. A., "Ductility of Concrete," International Symposium on Flexural Mechanics of Reinforced Concrete, Miami, FL, 1964.
22. Karsan, I. D., and Jirsa, J. O., "Behavior of Concrete under Compressive Loadings," *Journal of the Structural Division*, V. 95, No. 12, 1969, pp. 2543-2563.
23. Filippou, F. C.; Popov, E. P.; and Bertero, V. V., "Effects of Bond Deterioration on Hysteretic Behavior of Reinforced Concrete Joints," *Technical Report EERC 83-19*, University of California, Berkeley, Berkeley, CA, 1983.
24. Coleman, J., and Spacone, E., "Localization Issues in Force-Based Frame Elements," *Journal of Structural Engineering*, ASCE, V. 127, No. 11, 2001, pp. 1257-1265. doi: 10.1061/(ASCE)0733-9445(2001)127:11(1257)
25. Feenstra, P. H., "Computational Aspects of Biaxial Stress in Plain and Reinforced Concrete," Delft University of Technology, Delft, the Netherlands, 1993, 159 pp.